Lung ventilation estimation based on 4D-CT imaging

Sven Kabus[1], Jens von Berg[1], Tokihiro Yamamoto[2], Roland Opfer[1], and Paul J. Keall[2]

[1] Philips Research Europe – Hamburg, Germany
sven.kabus@philips.com *
[2] Department of Radiation Oncology, Stanford University School of Medicine, Stanford, CA, USA

Abstract. The estimation of lung ventilation would allow to prevent high functional lung regions from radiation injuries during radiation therapy of lung cancer. As 4D-CT images are a standard procedure for radiation therapy planning, the usage of these images for the additional lung ventilation estimation would be advantageous over other imaging methods specifically performed for ventilation estimation only. This would require both a registration of images of different respiratory phases yielding deformation vector fields and a suitable metric of ventilation estimation based on the deformation vector fields. We apply two different image registration methods and two different metrics to a set of 4D-CT images and compare them with each other and with a global reference measure based on independent lung volume measures from image segmentation.

1 Introduction

In radiation therapy planning of lung tumors it would be advantageous to consider spatial information of lung function (e.g., ventilation) to prevent high functional lung regions from radiation injury and achieve better quality of life. The current standard of care for ventilation assessment is nuclear medicine (NM) imaging [1, 2]. Recent techniques based on oxygen-enhanced magnetic resonance (MR) imaging utilize hyperpolarized noble gases (e.g., ^{129}Xe) [3, 4]. Images acquired with NM techniques suffer from a low spatial resolution. Also, for both of NM and MR techniques, there are issues including a long scan time, high costs, and low availability in radiotherapy departments. More recently, several groups [5–8] have employed four-dimensional (4D) CT images [9, 10] for ventilation assessment. Four-dimensional CT images for treatment planning can be used for ventilation assessment as well, thus not requiring any additional imaging sessions. Therefore, the 4D-CT-based approach potentially has several advantages over NM or MR technique as it is free, fast, available, and of high spatial resolution. However, the accuracy is dependent on image registration algorithms as

* We are grateful to an anonymous reviewer for helpul comments on our manuscript. Also, we thank Cristian Lorenz from Philips Research Europe – Hamburg for fruitful discussions.

well as of the metrics for ventilation. Several investigators demonstrated variations in registration results between algorithms [7, 11, 12]. In the previous work, we showed apparent discrepancies in deformation vector fields (DVFs) and ventilation images calculated by different registration algorithms [8]. There have been two different metrics used for ventilation assessment based on the DVFs. Guerrero et al. have employed difference in Hounsfield units (HU) as a metric of ventilation, and showed good agreements between global measures of ventilation (i.e., tidal volume) for patient data calculated using this method and those of manual measurements [6]. Reinhardt et al. have used the Jacobian determinant and demonstrated good agreements between local ventilation for sheep data determined by this approach and Xe-CT [5].

The contribution of the current work is to compare two different image registration methods with each other, both applied to 4D-CT and to also apply both of the reported metrics to estimate ventilation from the resulting DVFs on a set of four human 4D-CT scans. In addition, we compare our ventilation metrics with the relative change in lung volume for each phase transition taken from independent lung segmentation of each CT volume. Jacobian and relative volume change should be equal by definition – however, from a technical point of view this is not trivial and worth to show. Moreover, it can be considered as a necessary condition for a reliable ventilation estimation.

2 Methods

2.1 Data Sets and Image Acquisition

The 4D-CT scans were performed on the GE Discovery ST multislice PET/CT scanner (GE Medical Systems, Waukesha, WI) in cine mode at Stanford Cancer Center. Case 1 of the four examined cases was a patient with lung cancer, the other cases were breast cancer patients not showing lung metastases. During the CT scan, patient respiratory traces were acquired using the Varian RPM system (Varian Medical Systems, Palo Alto, CA), with the marker block placed on the upper abdomen. Scan parameters were set as follows: 0.5 s gantry rotation, 0.45 s cine interval, and 2.5 mm slice thickness. Each image reconstruction took 360 deg of data. The projection images were retrospectively sorted into ten respiratory phase-based bins of 3D CT image data (i.e., from 0% to 90% phase at 10% intervals). Figure 1 shows coronal views of two exemplary phases of Case 3 and all ten phase-to-phase subtraction images.

2.2 Registration Schemes

Given two reconstructed phases (one named reference phase, the other template phase in the following), image registration tries to find a deformation vector field $u : \mathbb{R}^3 \to \mathbb{R}^3$ such, that the displaced template phase is similar to the reference phase. In this work, two fundamentally different registration schemes have been

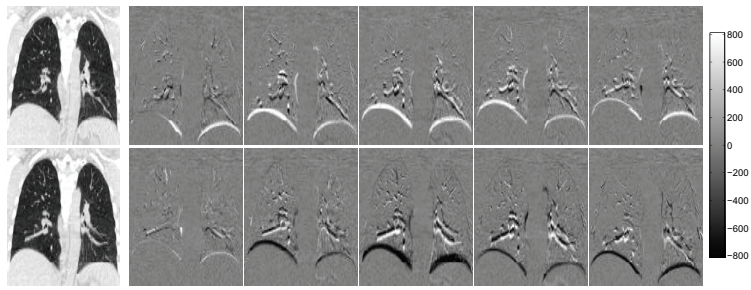

Fig. 1. Coronal views of reconstructed phases 30% and 80% (first column) and phase-to-phase subtraction images (remaining columns): row-wise are displayed $10\% - 0\%$, $20\% - 10\%$, ..., $0\% - 90\%$. Motion of diaphragm and vessel tree, particularly in the lower regions of the lung, is clearly visible. The change in sign for the diaphragm region occurs when changing from exhalation (0% to 60%) to inhalation (60% to 0%).

employed to estimate u. Whereas the first scheme matches surfaces (lung wall, vessel tree) followed by a thin-plate-spline interpolation to achieve the dense DVF, the second scheme is volumetric by itself.

2.3 Surface-based Registration

In the first, surface-based method we automatically determine the lung surface by a Hounsfield threshold at -650 HU and a marching cube triangulation in one phase. This surface not only covers the outer lung border but also the inner structures separating the parenchyma from the larger lung vessels. The number of triangles of this iso-surface ranges from 38,000 to 87,000. The method of deformable surface models [13] is now applied on this iso-surface of the lungs to adapt it to the second phase by minimizing the energy term $E = E_{ext} + \alpha E_{int}$. The external energy E_{ext} drives the mesh towards the surface points obtained in a surface detection step. The internal energy E_{int} restricts the flexibility by penalizing differences from the shape model. A number of such minimization steps is iteratively performed on the mesh. Details on the candidate point selection and on the calculation of the external energy can be found in [14]. The internal energy

$$E_{int} = \sum_{j} \sum_{k \in N(j)} \left((\mathbf{v}_j - \mathbf{v}_k) - s\mathbf{R}(\hat{\mathbf{v}}_j - \hat{\mathbf{v}}_k) \right)^2 \tag{1}$$

preserves shape similarity of all mesh vertices $\mathbf{v}_i$ to the model vertices $\hat{\mathbf{v}}_i$ from the initial iso-surface. $N(j)$ is the set of neighbors of vertex j. The neighboring vertices are those connected by a single triangle edge. The scaling factor s and the rotational matrix $\mathbf{R}$ are determined by a closed-form point-based registration method based on a singular value decomposition prior to calculation of (1) to

allow a similarity transformation (rigid transformation plus isotropic scaling) without effecting the internal energy.

By use of all vertex deformation vectors of the deformable surface, we construct a coarse displacement field for the lungs. Interpolation by thin-plate-splines on a subset of these vertices is used to create a dense field from it. The subset is obtained by replacing all vertices having a neighbor closer than 10 mm. Further details on this shape-tracking method, the impact of its parameters, and its computational performance are given in [14].

2.4 Volume-based Registration

The volumetric registration tries to find a DVF such, that the displaced template phase minimizes both a certain similarity measure $\mathcal{D}$ and a regularizing term $\mathcal{S}$. By adding a regularizing term, the registration problem is well-posed. For $\mathcal{D}$ we choose the popular sum of squared differences while for $\mathcal{S}$ an elastic regularizer [15] based on the Navier-Lamé equation is employed. The elastic regularizer assumes that the underlying images can be characterized as an elastic and compressible material. Its properties are modeled by the so-called Lamé constants λ, μ.

Based on calculus of variations we arrive at a system of non-linear partial differential equations to be solved,

$$\mu \Delta u + (\mu + \lambda) \nabla \cdot \nabla u = \nabla T_u (R - T_u) \; , \tag{2}$$

with T_u and R corresponding to the displaced template phase and the reference phase, respectively.

For the discretization of (2) finite differences in conjunction with Neumann boundary conditions have been chosen. The resulting system of linear equations consists on one hand of a sparse, symmetric and highly structured matrix arising from the regularizer and, on the other hand, of a so-called force vector corresponding to the similarity measure. By nature, the larger the contrast of misaligned image structures is, the larger the modulus of the force vector is. Therefore, in CT images bone structures get typically perfectly matched whereas soft tissue may be not aligned. This holds particularly for the lung-rib interface with on the one side the parenchyma following the breathing motion and on the other side the ribs staying in place or even moving in opposite direction. To circumvent mis-alignment of parenchymal structures we added a simple masking of the force vector. For every voxel with Hounsfield value above 0 HU in the reference phase, the force vector is set to zero for this voxel position. This results in a lung deformation which is not influenced by mis-alignment of the rib cage.

The corrected linear system of equations is then linearized and iteratively solved by a conjugate gradient scheme. The whole registration method is embedded into a multi-resolution setting (typical image pyramid has a resolution of $512 \times 512 \times 136$ at level 0, $256 \times 256 \times 136$ at level 1, $128 \times 128 \times 68$ at level 2 etc.; registration is executed on levels 4 to 1) and preceeded by an affine pre-registration.

3 Evaluation

For the datasets considered in this work no ground-truth such as nuclear medicine data or annotated landmark positions was available. But both registration methods have been previously validated with a method reported in [8]. For that validation similar CT scans with known annotated landmark positions were used. Unlike the current study, ten biphasic thorax CT data sets (max inhale and max exhale reconstructions only) were used. Two independent experts set corresponding landmark pairs (18–20 pairs) at vessel- and bronchi-bifurcations in all images. The landmark positions at one state were transformed using the DVFs obtained from the two registration methods and compared to the reference landmarks. For the validation the average Euclidean distance before and after registration have been compared. Given an average error of 5.99 mm ± 3.97 mm before registration, both methods showed a reduced error in all testcases (2.50 mm ± 2.16 mm for the surface-based method and 2.28 mm ± 1.87 mm for the volumetric method). Taking into account the relatively large difference between max inhale and max exhale state in that previous study, we expect a more accurate result and smaller registration errors for the consecutive registration in 10% steps given in the 4D-CT datasets investigated in this work.

To analyze the DVFs restricted to the lung, segmentation of the lung is required. For this purpose we use the segmentation scheme reported in [16]. The segmentation provides a binary mask of the lung but with the vessel tree excluded. To evaluate the segmentation result, we computed the total lung mass at each respiratory phase by integrating the density $\rho = (HU + 1000)/1000$ over the segmented lung. Then, the lung mass at each phase is subtracted from their mean (mean lung mass is 593 g, 558 g, 580 g, 628 g for patients 1 to 4, respectively). From these absolute differences, for patient 1 to 4 a mean error of 8.2 g ± 6.6 g, 11.0 g ± 4.5 g, 14.5 g ± 6.2 g, 6.5 g ± 3.7 g, respectively, result. Each DVF (restricted to those parenchyma voxels having a Hounsfield value above −1000 HU) is analyzed using the two different metrics:

1. **Jacobian analysis.** Given two phases, the corresponding DVF u maps each position in the reference phase onto the corresponding position in the template phase. Thus, the determinant of the Jacobian of $x + u(x)$ represents the local volume change at position x between reference phase and template phase,
$$\Delta V_{\mathrm{Jac}}(x) := \det(\nabla(x + u(x))) - 1\,. \tag{3}$$
A value of zero indicates local volume preservation whereas a positive (negative) value corresponds to local expansion (contraction).
2. **Hounsfield analysis.** Given two phases and the corresponding DVF u, a local change in lung volume can be estimated from the relative difference of corresponding Hounsfield values (cf. [6]). By denoting a Hounsfield value at position x in phase i as $HU_i(x)$ the metric is defined by
$$\Delta V_{\mathrm{HU}}(x) := 1000 \frac{HU_i(x + u(x)) - HU_{i+1}(x)}{HU_{i+1}(x)(HU_i(x + u(x)) + 1000)}\,. \tag{4}$$

Again, a positive (negative) value indicates local expansion (contraction). Note that the images have been smoothed with a Gaussian kernel before computing ΔV_{HU}.

Moreover, the lung segmentation [16] of each phase was used to compute the lung volume and from that the relative change in lung volume for each phase transition. This we took as a global reference value for our volume change estimates.

4 Results

Without any further parameter tuning, both methods have been successfully applied to the four patient cases with ten phases each. The quality of registration has been assessed by visually inspecting each residual image (i.e., the subtraction image obtained after registration). Almost all registrations indicate an optimal match of lung wall and diaphragm. In addition, in most cases the vessel-tree has been correctly aligned. The results for method 2 are slightly better than for method 1 which can be explained by the volumetric nature of method 2 (see Figure 2 for an exemplary view). For outer-lung regions such as spine or rib cage the residual images from both methods indicate a worse alignment compared to the subtraction images obtained before registration (compare with Figure 1). This is based in method 1 on the extraction of the lung surface only and in method 2 on the threshold applied on the force vector.

According to Section 3 the resulting DVFs are analyzed using two different metrics to estimate the local change in lung volume (see second and third column of Figure 2 for exemplary views). By using the lung segmentation of each phase, the values ΔV_{Jac} and ΔV_{HU} are integrated within the lung (displayed in Figure 3). Dependent on the patient case these relative volume changes lie between -7% for exhalation and $+11\%$ for inhalation.

Finally, the volume change estimates from both registration methods and both analysis metrics are compared with our global reference segmentation (depicted red in Figure 3). A quantitative comparison is provided by Table 1. Here, for each registration method and each analysis metric the absolute difference between estimated volume change and segmentation-based volume change is given in percentage. Overall, the Jacobian analysis yields an error in volume change estimation of 0.8% and 0.4% for method 1 and 2, respectively, while the estimation error of the Hounsfield analysis is larger (1.4% and 0.9%).

5 Discussion and Conclusion

We have applied two fully independent image registration methods to 4D-CT lung scans. The resulting DVFs for each phase-to-phase transition are analyzed with two different metrics in order to estimate local lung ventilation. An overall inspection reveals similar estimates of Jacobian and Hounsfield analysis.

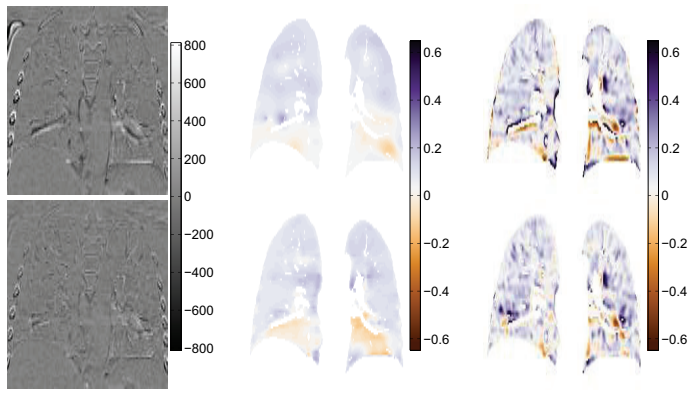

Fig. 2. For the same coronal view as in Figure 1, residual (left), Jacobian analysis (center), and Hounsfield analysis (right) are investigated after registration of 90% onto 80% phase with method 1 (top) and method 2 (bottom). Note that the two metrics are analyzed and visualized within the lung only – white regions belong to either the vessel tree or are outside the lung.

For a quantitative inspection we integrated these estimates over the lung and compared this estimated change of lung volume to that arising from an independent lung segmentation. Our results show that for both registration methods the volume change estimated by Jacobian analysis agrees well with the segmentation-based volume change (mean deviation of 0.8% and 0.4%). The Hounsfield analysis as the second investigated metric indicates a less optimal result (mean deviation of 1.4% and 0.9%). Since this metric is sensitive to local changes in the DVF but also to imaging- or reconstruction-related artifacts, a concluding rating is difficult. For a deeper insight, beside the global comparisons a point-based comparison between Jacobian and Hounsfield analysis seems to be worthwhile.

Table 1. Mean and standard deviation of absolute difference (in %) between estimated volume change and segmentation-based volume change.

Case	Jacobian analysis		Hounsfield analysis	
	method 1	method 2	method 1	method 2
1	0.84 ± 0.75	0.54 ± 0.48	1.75 ± 1.57	1.26 ± 1.59
2	0.74 ± 0.48	0.47 ± 0.42	1.29 ± 1.55	1.08 ± 1.04
3	1.09 ± 0.61	0.26 ± 0.29	1.59 ± 1.09	0.70 ± 0.94
4	0.50 ± 0.29	0.35 ± 0.25	0.91 ± 0.72	0.54 ± 0.50
mean	0.79 ± 0.53	0.41 ± 0.36	1.38 ± 1.23	0.89 ± 1.02

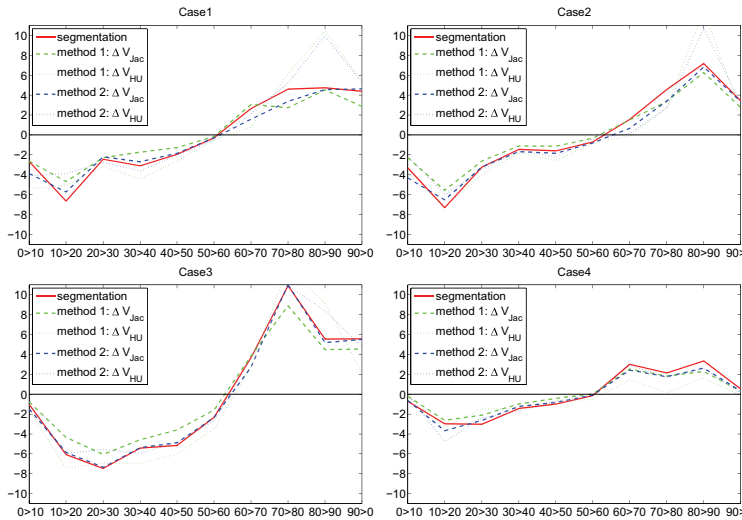

Fig. 3. Volume changes (in %) for each patient case and for each phase-to-phase transition obtained by either Jacobian analysis (dashed) or HU subtraction analysis (dotted) for method 1 (green) and method 2 (blue). For comparison, the volume change derived by a lung segmentation is depicted (red).

References

1. Suga, K.: Technical and analytical advances in pulmonary ventilation SPECT with Xenon-133 gas and Tc-99m-Technegas. Ann Nucl Med **16**(5) (2002) 303–10
2. Harris, R.S., Schuster, D.P.: Visualizing lung function with positron emission tomography. J Appl Physiol **102**(1) (2007) 448–58
3. Kauczor, H.U., Hanke, A., Van Beek, E.J.: Assessment of lung ventilation by MR imaging: current status and future perspectives. Eur Radiol **12**(8) (2002) 1962–70
4. Fain, S.B., Korosec, F.R., Holmes, J.H., O'Halloran, R., Sorkness, R.L., Grist, T.M.: Functional lung imaging using hyperpolarized gas MRI. J Magn Reson Imaging **25**(5) (2007) 910–23
5. Reinhardt, J.M., Christensen, G.E., Hoffman, E.A., Ding, K., Cao, K.: Registration-derived estimates of local lung expansion as surrogates for regional ventilation. Inf Process Med Imaging **20** (2007) 763–74
6. Guerrero, T., Sanders, K., Castillo, E., Zhang, Y., Bidaut, L., Pan, T., Komaki, R.: Dynamic ventilation imaging from four-dimensional computed tomography. Phys Med Biol **51**(4) (2006) 777–91
7. Yaremko, B.P., Guerrero, T.M., Noyola-Martinez, J., Guerra, R., Lege, D.G., Nguyen, L.T., Balter, P.A., Cox, J.D., Komaki, R.: Reduction of normal lung irradiation in locally advanced non-small-cell lung cancer patients, using ventila-

tion images for functional avoidance. Int J Radiat Oncol Biol Phys **68**(2) (2007) 562–71
8. Vik, T., Kabus, S., von Berg, J., Ens, K., Dries, S., Klinder, T., Lorenz, C.: Validation and comparison of registration methods for free-breathing 4D lung CT. In: Proc. of SPIE Medical Imaging. Volume 6914., SPIE (2008) 69142P–1–69142P–10
9. Keall, P.J., Starkschall, G., Shukla, H., Forster, K.M., Ortiz, V., Stevens, C.W., Vedam, S.S., George, R., Guerrero, T., Mohan, R.: Acquiring 4D thoracic CT scans using a multislice helical method. Phys Med Biol **49**(10) (2004) 2053–67
10. Rietzel, E., Pan, T., Chen, G.T.: Four-dimensional computed tomography: image formation and clinical protocol. Med Phys **32**(4) (2005) 874–89
11. Kashani, R., Hub, M., Kessler, M.L., Balter, J.M.: Technical note: a physical phantom for assessment of accuracy of deformable alignment algorithms. Med Phys **34**(7) (2007) 2785–8
12. Brock, K.K.: A multi-institution deformable registration accuracy study. Int J Radiat Oncol Biol Phys **69**(3) (2007) S44
13. Weese, J., Kaus, M., Lorenz, C., Lobregt, S., Truyen, R., Pekar, V.: Shape constrained deformable models for 3D medical image segmentation. In: Proc. of IPMI, Springer–Verlag (2001) 380–387
14. von Berg, J., Barschdorf, H., Blaffert, T., Kabus, S., Lorenz, C.: Surface based cardiac and respiratory motion extraction for pulmonary structures from multiphase CT. In: Proc. of SPIE Medical Imaging. Volume 6511., SPIE (2007) 65110Y
15. Broit, C.: Optimal Registration of Deformed Images. PhD thesis, University of Pennsylvania (1981)
16. Wiemker, R., Opfer, R., Bülow, T., Rogalla, P., Steinberg, A., Dharaiya, E., Subramanyan, K.: Towards computer aided emphysema quantification on ultra-low-dose CT: Reproducibility of ventrodorsal gravity effect measurement and correction. In: Proc. of SPIE Medical Imaging. Volume 6514., SPIE (2007) 65140O